

Diagnosing ratio of electron density to collision frequency of plasma surrounding scaled model in a shock tube using low-frequency alternating magnetic field phase shift

Ming-Xing Wu, Kai Xie, Yan Liu, Han Xu, Bao Zhang, and De-Yang Tian

Citation: Chin. Phys. B, 2024, 33 (**5**): 055204. DOI: 10.1088/1674-1056/ad2d56
Journal homepage: http://cpb.iphy.ac.cn; http://iopscience.iop.org/cpb

What follows is a list of articles you may be interested in

Characteristics of the electromagnetic wavepropagation inmagnetized plasma sheath and practical methodfor blackout mitigation

Xiang Wu(吴翔), Jiahui Zhang(张珈珲), Guoxiang Dong(董果香), and Lei Shi(石磊)
Chin. Phys. B, 2024, 33 (**5**): 055201. DOI: 10.1088/1674-1056/ad24d4

Hollow cathode effect in radio frequency hollow electrode discharge in argon

Liu-Liang He(贺柳良), Feng He(何锋), and Ji-Ting Ouyang(欧阳吉庭)
Chin. Phys. B, 2024, 33 (**3**): 035203. DOI: 10.1088/1674-1056/ad1a89

Transition from a filamentary mode to a diffuse one with varying distance from needle to stream of an argon plasma jet

Hui-Min Xu(许慧敏), Jing-Ge Gao(高敬格), Peng-Ying Jia(贾鹏英), Jun-Xia Ran(冉俊霞), Jun-Yu Chen(陈俊宇), and Jin-Mao Li(李金懋)
Chin. Phys. B, 2024, 33 (**1**): 015205. DOI: 10.1088/1674-1056/ad0149

Fluid-chemical modeling of the near-cathode sheath formation process in a high current broken in DC air circuit breaker

Shi-Dong Peng(彭世东), Jing Li(李静), Wei Duan(段薇), Yun-Dong Cao(曹云东), Shu-Xin Liu(刘树鑫), and Hao Huang(黄浩)
Chin. Phys. B, 2024, 33 (**1**): 015204. DOI: 10.1088/1674-1056/acd7cb

Effect of sharp vacuum-plasma boundary on the electron injection and acceleration in a few-cycle laser driven wakefield

Guo-Bo Zhang(张国博), Song Liu(刘松), De-Bin Zou(邹德滨), Ye Cui(崔野), Jian-Peng Liu(刘建鹏), Xiao-Hu Yang(杨晓虎), Yan-Yun Ma(马燕云), and Fu-Qiu Shao(邵福球)
Chin. Phys. B, 2023, 32 (**9**): 095202. DOI: 10.1088/1674-1056/acdc0c

---

Diagnosing ratio of electron density to collision frequency of plasma surrounding scaled model in a shock tube using low-frequency alternating magnetic field phase shift

Ming-Xing Wu(吴明兴)[1], Kai Xie(谢楷)[1,†], Yan Liu(刘艳)[1], Han Xu(徐晗)[1], Bao Zhang(张宝)[1], and De-Yang Tian(田得阳)[2]

[1] *School of Aerospace Science and Technology, Xidian University, Xi'an* 710071, *China*
[2] *Hypervelocity Aerodynamics Institute, China Aerodynamics Research and Development Center, Mianyang* 621000, *China*

(Received 8 December 2023; revised manuscript received 7 February 2024; accepted manuscript online 27 February 2024)

A non-contact low-frequency (LF) method of diagnosing the plasma surrounding a scaled model in a shock tube is proposed. This method utilizes the phase shift occurring after the transmission of an LF alternating magnetic field through the plasma to directly measure the ratio of the plasma loop average electron density to collision frequency. An equivalent circuit model is used to analyze the relationship of the phase shift of the magnetic field component of LF electromagnetic waves with the plasma electron density and collision frequency. The applicable range of the LF method on a given plasma scale is analyzed. The upper diagnostic limit for the ratio of the electron density (unit: m^{-3}) to collision frequency (unit: Hz) exceeds 1×10^{11}, enabling an electron density to exceed 1×10^{20} m^{-3} and a collision frequency to be less than 1 GHz. In this work, the feasibility of using the LF phase shift to implement the plasma diagnosis is also assessed. Diagnosis experiments on shock tube equipment are conducted by using both the electrostatic probe method and LF method. By comparing the diagnostic results of the two methods, the inversion results are relatively consistent with each other, thereby preliminarily verifying the feasibility of the LF method. The ratio of the electron density to the collision frequency has a relatively uniform distribution during the plasma stabilization. The LF diagnostic path is a loop around the model, which is suitable for diagnosing the plasma that surrounds the model. Finally, the causes of diagnostic discrepancy between the two methods are analyzed. The proposed method provides a new avenue for diagnosing high-density enveloping plasma.

Keywords: low-frequency alternating magnetic field phase shift, shock-tube plasma diagnosis, electron density, collision frequency

PACS: 52.70.–m, 52.70.Ds, 52.40.Db, 07.55.Nk **DOI:** 10.1088/1674-1056/ad2d56

1. Introduction

Shock tubes are hypersonic flow field simulation devices frequently used in ground experiments. Built-in scaled models in shock tubes are important research tools that have rapidly advanced in the fields of near-space hypersonic aircraft target characteristics, communication interruptions, and plasma flow control.[1–6] It is crucial to obtain the electron density and collision frequency distribution of plasma in such work. Over the past decade, the propagation of low-frequency (LF) electromagnetic waves in plasma surrounding a model has attracted much attention.[7–13] LF refers to electromagnetic wave frequencies that are much lower than the plasma frequency, and the motion of charged particles at such frequencies can be approximated as conduction current. When LF waves are incident on an enveloping plasma, a closed current loop forms on the surface of the plasma. As the conduction current is much greater than the displacement current, the plasma is equivalent to a loop resistance,[14] which closely relates to the ratio of the plasma electron density (n_e) to collision frequency (ν_e). Therefore, directly obtaining the n_e/ν_e values within the plasma proves more convenient for studying the characteristics of LF wave propagation in plasma whereas predetermining the n_e/ν_e values provides references for subsequent research on enveloping plasma non-contact diagnostic methods.

However, there is no direct non-contact method available for obtaining n_e/ν_e values of the enveloping plasma of a shock tube. In general, shock-tube plasma has an electron density ranging from 10^9 cm^{-3} to 10^{13} cm^{-3}, a collision frequency ranging from 1 GHz to 100 GHz, and a duration of only tens of microseconds. The diagnosis of shock-tube plasma thus requires a method having a wide dynamic range and precise time resolution. At present, in the methods commonly used to obtain the shock-tube plasma electron density and collision frequency, the Langmuir electrostatic probes and microwaves are adopted.

The electrostatic probe method[15–18] is straightforward and portable and has a time resolution better than 1 μs and a measurement dynamic range spanning nearly three orders of magnitude. The electron density and electron temperature can be calculated through measuring the voltammetry characteristic curve by using probes, and the collision frequency can be obtained from an empirical formula.[19] However, the insertion of electrostatic probes inevitably disturbs the flow field. Mean-

†Corresponding author. E-mail: kaixie@mail.xidian.edu.cn
© 2024 Chinese Physical Society and IOP Publishing Ltd

while, the surface material of the electrostatic probe tends to undergo ablating and spalling when exposed to the impact of hot airflow, leading to compromised functionality and potential misdiagnosis.

The microwave interferometry and the transmission methods[20–24] obtain the average electron density on the propagation path and have the advantages of not interfering with the flow field, a wide dynamic range, and a precise time resolution. Among these methods, microwave interferometry measures the phase difference between the signal transmitted through the plasma and the reference signal without plasma.[20] Microwave interferometry calculates the electron density through adopting microwave propagation phase difference. However, the plasma collision frequency cannot be obtained from the phase shift alone. Microwave interferometry is thus unsuitable for obtaining n_e/ν_e values. The microwave transmission method is used to measure the attenuation and phase shift of the transmitted signal. By combining the attenuation and phase shift with the characteristics of the plasma medium, it is possible to obtain the electron density and collision frequency separately.[21] However, when using the microwave transmission method to diagnose the plasma surrounding a model, the accuracy of the diagnostic method heavily relies on the main beam alignment of transceiver antennas. This requires the transceiver antenna to have a narrow beam and strong directivity. In addition, it requires the receiving antenna to be installable in a small model. However, it is usually a challenge to design narrow-beam antennas that satisfy the requirements of diagnostic experiments. Therefore, both the electrostatic probe and microwave method have limitations in diagnosing the plasma that surrounds the shock tube built-in model.

Our recent theoretical and experimental studies reported the characteristics of the propagation of LF electromagnetic waves through shock-tube plasma.[10–13] When LF electromagnetic wave is incident on the plasma, the magnetic field component of the LF electromagnetic wave induces a current in the plasma. The magnetic field generated by the induced current offsets the original incident magnetic field. This mechanism enables the alternating magnetic field component to transmit high density and collision plasma with low attenuation while inducing a phase shift. We found that the attenuation and phase shift both strongly correlate with the incident wave frequency, the route of the induced current, and the value of n_e/ν_e. It is thus possible to directly obtain the values of n_e/ν_e according to the relationship between the LF alternating magnetic field phase shift and plasma parameters. In addition, owing to low attenuation at LF in high density and collision plasma, this method may have a wide diagnostic range.

This work introduces a novel contactless LF diagnostic method for the plasma surrounding shock-tube built-in scaled models. The proposed method enables the direct measurement of the electron-density-to-collision-frequency ratio along the plasma loop path. The relationship between the LF phase shift and plasma parameters is analyzed and used for diagnosing shock-tube plasma, and the application range of the LF diagnostic method is analyzed. Furthermore, LF diagnostic experiments on a shock tube are conducted to validate the proposed method. The findings of the study are important to both theoretical plasma research and engineering applications.

The remainder of the paper is arranged as follows. In Section 2, the mathematical derivation of the LF diagnosis method is described. In Section 3, the theoretical analysis of the LF diagnosis method is presented. In Section 4, the experimental results are given and discussed. Finally, some conclusions are drawn from the present study in Section 5.

2. LF diagnostic theoretical analysis

According to the theory of the propagation of electromagnetic waves in plasma,[25] plasma is a lossy dispersive medium with the equivalent dielectric constant

$$\varepsilon_r = 1 - \frac{\omega_p^2}{\omega(\omega - \mathrm{j}\nu_{en})} = 1 - \frac{\omega_p^2}{\omega^2 + \nu_{en}^2} - \mathrm{j}\frac{\nu_{en}}{\omega}\frac{\omega_p^2}{\omega^2 + \nu_{en}^2}, \quad (1)$$

where ω is the angular frequency of incident wave, ν_{en} is the collision angular frequency, ω_p is the plasma frequency, and the ω_p and electron density n_e are related by

$$\omega_p = \sqrt{\frac{n_e e^2}{\varepsilon_0 m_e}}, \quad (2)$$

with e being the unit charge, m_e the electron's mass, and ε_0 the permittivity of free space. In electromagnetic wave theory, the conductivity σ and relative dielectric constant ε_r are related by

$$\varepsilon_r = 1 - \frac{\omega_p^2}{\nu_{en}^2} - \mathrm{j}\frac{\sigma}{\omega\varepsilon_0}. \quad (3)$$

By comparing Eq. (1) with Eq. (3), the conductivity is obtained as

$$\sigma = \frac{\varepsilon_0 \nu_{en} \cdot \omega_p^2}{\omega^2 + \nu_{en}^2}. \quad (4)$$

At LF, $\omega \ll \omega_p$, $\omega \ll \nu_{en}$, σ can be further simplified into

$$\sigma \approx \frac{\varepsilon_0 \omega_p^2}{\nu_{en}} = \frac{e^2 n_e}{m_e \nu_{en}}. \quad (5)$$

In the case of enveloping plasma, the propagation characteristics of LF electromagnetic wave can be analyzed by adopting electromagnetic interference (EMI) theory. At LF, the plasma is electrically small, and the electric and magnetic field components of the electromagnetic wave can be considered separately.[14] When an LF alternating magnetic field is incident on the plasma, the plasma induces a magnetic field whose direction is opposite to that of the original magnetic field, thereby causing the attenuation and phase shift of the original magnetic field. This process is illustrated in Fig. 1.

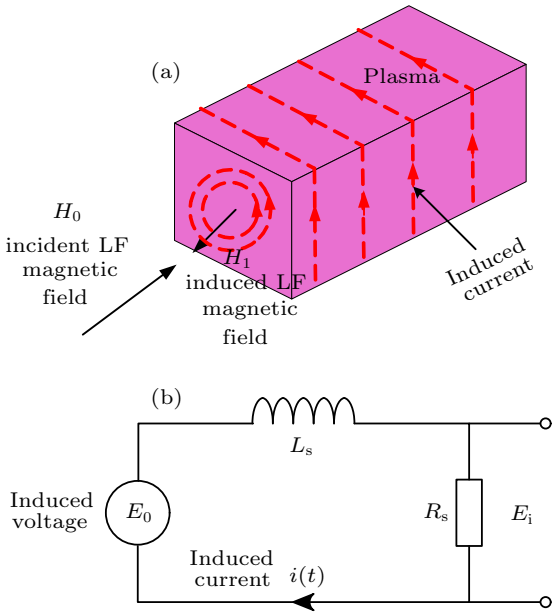


Fig. 1. Equivalent circuit model of LF alternating magnetic field incident on plasma: (a) schematic diagram of plasma shield structure and (b) equivalent circuit.

In Fig. 1, E_0 is the induced voltage in a loop on the plasma surface, L_s is the equivalent inductance of the loop, and R_s is the equivalent resistance of the loop. The induced voltage E_0 is given by[26]

$$E_0 = -\frac{\mathrm{d}}{\mathrm{d}t}\int \mu_0 H_0 \,\mathrm{d}s = -\mathrm{j}\omega\mu_0 H_0 A, \tag{6}$$

where ω is the angular frequency of incident wave, μ_0 is the permeability of a vacuum, and A is the plasma shield cross-sectional area. Denoting the original incident magnetic field as H_0, the induced current $i(t)$ in the equivalent circuit is

$$i(t) = \frac{E_0}{R_s + \mathrm{j}\omega L_s} = \frac{-\mathrm{j}\omega\mu_0 A H_0}{R_s + \mathrm{j}\omega L_s}. \tag{7}$$

Denoting the magnetic field transmitted through the plasma shield as H_i, the induced voltage E_i is expressed as

$$E_i = -\mathrm{j}\omega\mu_0 A H_i = i(t) R_s = \frac{E_0 \cdot R_s}{R_s + \mathrm{j}\omega_c L_s}. \tag{8}$$

Combining Eqs. (6) and (8) gives the transmitted LF alternating magnetic field as

$$H_i = H_0 \frac{R_s}{R_s + \mathrm{j}\omega L_s}. \tag{9}$$

Therefore, the transmission coefficient T of an LF alternating magnetic field passing through the plasma is

$$T = \frac{H_i}{H_0} = \frac{R_s}{R_s + \mathrm{j}\omega L_s}. \tag{10}$$

The inductive impedance is the main impedance of the loop when an LF alternating magnetic field is incident on the plasma. The induced current $i(t)$ generates a magnetic field with a direction opposite to that of the incident magnetic field, thereby canceling out part of the magnetic field within the plasma. The degree of cancelation relates to the incident angular frequency ω, plasma equivalent loop resistance R_s, and loop inductance L_s. The R_s inductance and L_s are determined by some factors such as the shape and size of the plasma.

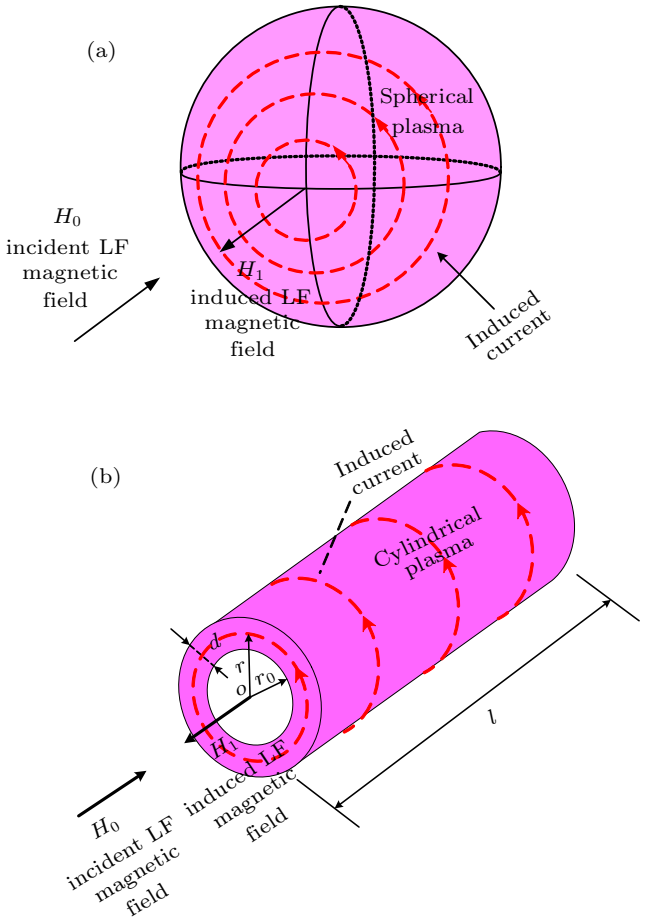


Fig. 2. Enveloping plasma shapes: (a) spherical plasma and (b) cylindrical plasma.

For example, L_s and R_s of the spherical shell plasma in Fig. 2(a) are respectively[27]

$$L_s = \frac{2\pi\mu_0 r n^2}{9}, \quad R_s = \frac{2\pi n^2}{3d\sigma}, \tag{11}$$

where r is the radius of the plasma sphere, d is the thickness of the plasma shell, σ is the equivalent conductivity of the plasma, and n is the equivalent number of turns. By inserting Eq. (11) into Eq. (10), the transmission coefficient of the LF alternating magnetic field passing through the plasma shell is obtained as

$$T = \frac{R_s}{R_s + \mathrm{j}\omega L_s} = \frac{1}{1 + \mathrm{j}\omega\mu_0 r d\sigma/3}. \tag{12}$$

The relationship between the attenuation and phase shift and the ratio of the plasma electron density to collision frequency (n_e/ν_e) are further obtained by combining Eqs. (5) and (12) as

$$\begin{cases} \mathrm{Att} = 20\log_{10}\left|1\Big/\sqrt{1+\left(\eta\dfrac{n_e}{\nu_e}\right)^2}\right|, \\ \Delta\varphi = -\arctan\left(\eta\dfrac{n_e}{\nu_e}\right) - \varphi_0, \end{cases} \quad \eta = \frac{\omega\mu_0 r d e^2}{6\pi m_e}. \tag{13}$$

In the example of the cylindrical plasma in Fig. 2(b), L_s and R_s are

$$L_s = \frac{n^2 \mu_0 \pi r^2}{l}, \quad R_s = \frac{2\pi r n^2}{dl\sigma}, \tag{14}$$

where l is the length of the cylindrical plasma, r is the radius of the plasma, d is the thickness of the plasma, n is the number of equivalent turns, and σ is the equivalent conductivity of the plasma. When the spatial distributions of the plasma parameters are uniform, the induction path can be equivalently represented by the path located in the center of the plasma, and we thus have $r = r_0 + d/2$. By inserting Eq. (14) into Eq. (10), the transmission coefficient of the LF alternating magnetic field passing through the cylindrical plasma is obtained as

$$T = \frac{R_s}{R_s + j\omega L_s} = \frac{1}{1 + j\omega\mu_0 r d\sigma/2}. \tag{15}$$

Furthermore, the attenuation and phase shift are given by

$$\begin{aligned} &\mathrm{Att} = 20\log_{10}\left|1\Big/\sqrt{1+\left(\xi\frac{n_e}{\nu_e}\right)^2}\right|, \\ &\Delta\varphi = -\arctan\left(\xi\frac{n_e}{\nu_e}\right) - \varphi_0, \\ &\xi = \frac{\omega\mu_0 r d e^2}{4\pi m_e}. \end{aligned} \tag{16}$$

Equations (13) and (16) show that no matter whether the enveloping plasma is spherical or cylindrical, the attenuation and phase shift of the LF alternating magnetic field relate to n_e/ν_e. The rectangular enveloping plasma in Fig. 1(a) can be equivalently represented as a cylinder with the same circumference as the rectangle, and L_s and R_s can be obtained from Eq. (14),[28] which ultimately gives the transmission coefficient. Furthermore, for any shaped electrically small enveloping plasma, if the equivalent loop inductance and loop resistance are determined, the equivalent circuit method can be used to obtain the LF transmission coefficient. Therefore, the transmission coefficient of an arbitrarily shaped enveloping plasma transmitted by an LF alternating magnetic field is expressed as

$$T = f(n_e/\nu_e, \xi), \tag{17}$$

where ξ is determined by the incident LF and the plasma shape dimension. Under any enveloping plasma, the LF phase shift can also be expressed as a function of n_e/ν_e

$$\Delta\varphi = g(n_e/\nu_e, \xi). \tag{18}$$

As long as n_e/ν_e is obtained, the phase characteristics of the LF alternating magnetic field passing through the plasma can be calculated by using an equivalent circuit. Conversely, n_e/ν_e can be diagnosed by using the LF phase characteristic formula (18). In this work, the cylindrical shock-tube plasma is taken for example and analyzed by using the cylindrical enveloping plasma model.

3. Analysis of LF diagnostic method

The attenuation and phase shift of an LF alternating magnetic field are affected by the plasma geometry, size, electron density, and collision frequency. The diagnostic of plasma parameters demands a small attenuation of the incident magnetic field and for the phase shift to effectively reflect variation in the plasma state. According to Eqs. (13) and (16), as the phase approaches 90°, n_e/ν_e tends to infinity, and the inverse solution method is inapplicable. It is thus necessary to estimate the relationship between the incident wave and plasma state before performing inversion. For a more intuitive analysis, the attenuation and phase shift introduced by different plasma characteristics are calculated by adopting EMI theory (Eq. (15)) and CST Studio Suite (CST), which is a professional electromagnetic simulation software.

Figure 3 illustrates the CST simulation model with parameter settings of a wall thickness $a = 20$ mm, plasma thickness $d = 25$ mm, missile body model radius $r = 15$ mm, and length $l = 200$ mm. The electron density (n_e) ranges from 5×10^{16} m^{-3} to 5×10^{19} m^{-3}, the collision frequency (ν_e) is set to 5 GHz, 10 GHz, 50 GHz, and 100 GHz, and n_e/ν_e ranges from 5×10^5 to 1×10^{10}. Open boundary conditions are used, and plane waves are radiated from the far field region, sequentially incident on the Teflon shock tube wall and plasma layer, and finally reach the center of the LF probe. Since the influence of the plasma layer on the magnetic field component of the electromagnetic wave is considered, only the magnetic field strength and phase at the surface of the LF probe are recorded. Similar simulation is conducted while the plasma layer is replaced by air. By comparing the magnetic field strengths and phases under these two conditions, the relative attenuation and phase shift caused by plasma can be obtained. The results of the attenuation and phase shift calculations are shown in Figs. 4 and 5, respectively.

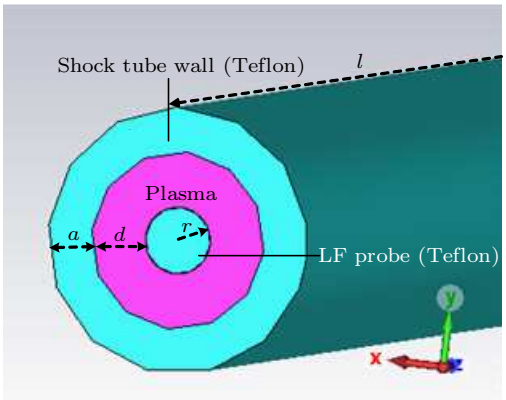


Fig. 3. Plasma LF alternating magnetic field propagation model in CST software.

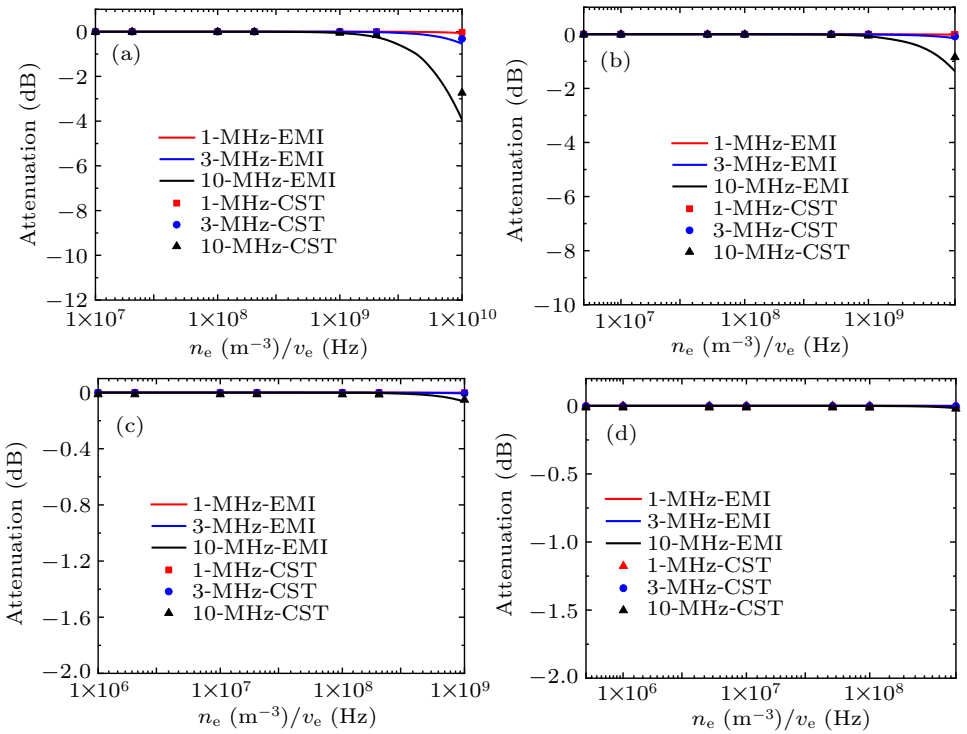


Fig. 4. Attenuations of LF alternating magnetic fields having frequencies of 1 MHz, 3 MHz, and 10 MHz at collision frequencies: v_e = 5 GHz (a), 10 GHz (b), 50 GHz (c), and 100 GHz (d).

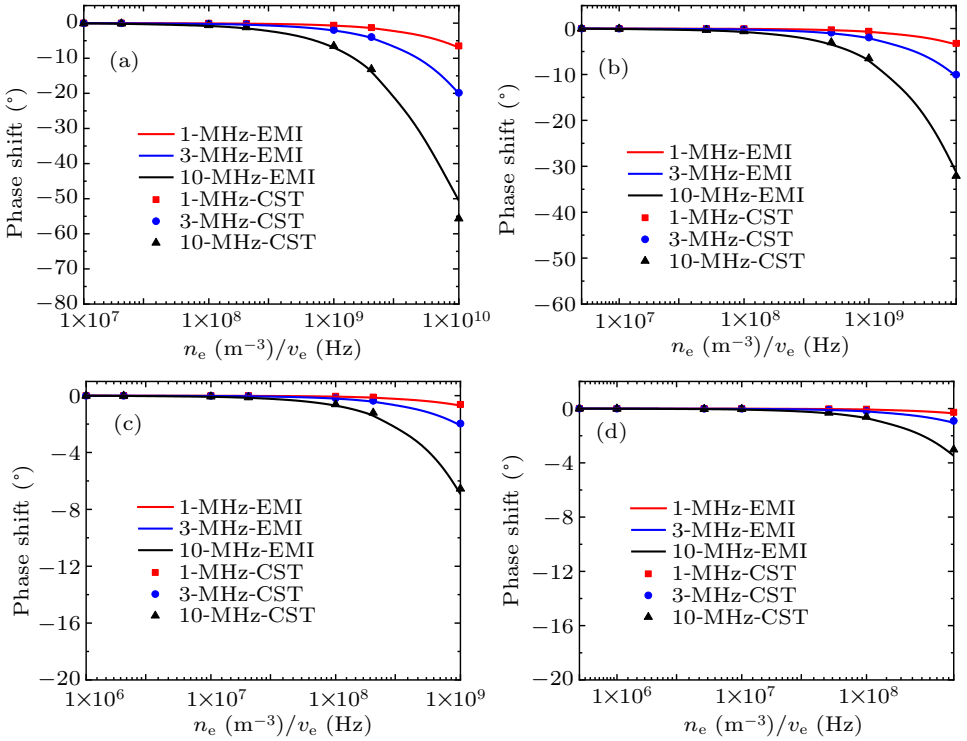


Fig. 5. Phase shifts of LF alternating magnetic fields having frequencies of 1 MHz, 3 MHz, 10 MHz at collision frequencies: v_e = 5 GHz (a), 10 GHz (b), 50 GHz (c), and 100 GHz (d).

Figures 4 and 5 show that the results of the theoretical computation and CST simulation are well consistent in the specific ranges of the electron density and collision frequency. At $n_e/v_e = 1 \times 10^{10}$, there is a deviation between the value of 10 MHz obtained by EMI theoretical calculation and the CST simulation value. This deviation is due to the EMI theoretical calculation selecting an induction path passing through the middle of the plasma. As the conductivity increases, the skin effect strengthens, causing the induction path to shift and generate errors, but the errors are still within a small range. The attenuation and phase shift have a nearly-linear correlation with the given values of n_e/v_e, validating the accuracy

of the theoretical calculation model. When the LF wave is not attenuated, the phase shift has already occurred. When the collision frequency is constant, the phase shift of the alternating magnetic field at the three frequencies gradually increases with the electron density increasing. The phase shift becomes more pronounced when n_e/v_e exceeds 1×10^8. At n_e/v_e less than 1×10^8, the plasma parameter changes slightly, and the phase shift changes at 1 MHz, 3 MHz, and 10 MHz are small. For all plasma states, the maximum phase shift of the LF is 55°, which still falls within the effective linear range. Under typical experimental conditions, a shock tube generates plasma with an electron density exceeding 10^{19} m^{-3} and a collision frequency of a few tens of GHz. Generally, n_e/v_e for shock-tube plasma exceeds 1×10^8. The plasma states adopted in simulation analysis cover the typical range of shock-tube plasma parameters. Nevertheless, the simulation results clearly indicate that the attenuation of LF magnetic field waves is no more than 10 dB, and the fluctuation in the LF magnetic field phase shift meets the requirements for shock plasma diagnostics. It is evident that the LF phase shift can be used for diagnosing shock-tube plasma. In experiment, only the phase shift of the LF alternating magnetic field having passed through the plasma needs to be recorded, when the plasma size and incident wave frequency are known. The n_e/v_e values are directly determined.

As the phase shift and n_e/v_e solved by the equivalent circuit method are arctan functions, as n_e/v_e increases infinitely, the phase shift only approaches 90° indefinitely. In this case, the phase shift does not reflect the change in n_e/v_e. We set the linear interval of the phase shift change as [0°, 80°], with values beyond 80° being invalid. The two-dimensional distribution of the LF alternating magnetic field phase shift with electron density and collision frequency is calculated by adopting the equivalent circuit method, and the results are presented in Fig. 6. In the figure, the contours of the LF magnetic field phase shift coincides with those of n_e/v_e, indicating that the phase shift is a function of n_e/v_e. At low electron density or a high collision frequency, the LF magnetic field phase shift is smaller. At an electron density of 5×10^{19} m^{-3} and a collision frequency of 1 GHz, the phase shifts of 1-, 3-, and 10-MHz alternating magnetic fields are 31.30°, 61.40°, and 80.8°, respectively. At this point, the 10-MHz phase shift exceeds the critical value. The upper diagnostic limits of the three frequencies are 4.67×10^{11}, 1.56×10^{11}, and 4.67×10^{10}, respectively. The upper limit of n_e/v diagnosis can thus be improved by reducing the incidence frequency. On a given plasma scale, the phase shift is inversely proportional to the collision frequency and directly proportional to the electron density, and the upper limit of LF diagnosis exceeds 1×10^{11}, the corresponding electron density exceeds 1×10^{20} m^{-3}, and the collision frequency is lower than 1 GHz.

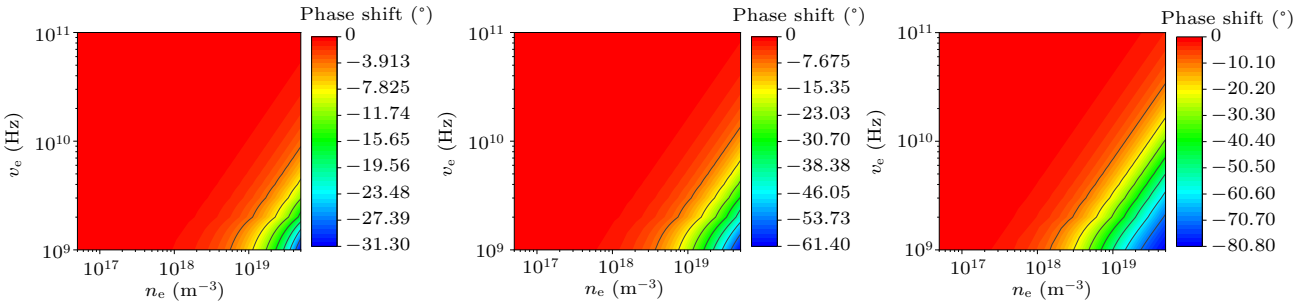


Fig. 6. Two-dimensional diagram of phase shifts of LF alternating magnetic fields at frequencies of 1 MHz (a), 3 MHz (b), and 10 MHz (c).

4. Experiment and discussion

4.1. Principle and setup of electrostatic probe method

Electrostatic probe method is commonly used for diagnosing shock tube plasma. In this work, a dual-probe measurement method was used, and its circuit schematic diagram is shown in Fig. 7(a).

The V_D and I_D are the operating voltage and current between the two probes, while the volt–ampere characteristic curve is shown in Fig. 7(b). Assuming that the two probes are exactly the same, i.e., they have the same collection area and equal electron saturation current and ion saturation current, equation (19) can be obtained as follows:

$$I_D = I_{e1} - I_{si} = I_{si} - I_{e2},$$

$$\begin{aligned} V_D &= V_+ - V_-, \\ V_C &= \phi_{p1} - \phi_{p2}, \\ I_{e1} &= I_{se}\exp\left[e\left(V_+ - \phi_{p1}\right)/k_B T_e\right], \end{aligned} \tag{19}$$

where V_+ and V_- are the potentials at the ends of the two probes, ϕ_{p1} and ϕ_{p2} are the plasma potentials in the space where the probes are located, I_{e1} and I_{e2} are the electron currents collected by the two probes, I_{se} is the electron saturation current, and I_{si} is the ion saturation current. In the experiment, the two probes are very close to each other, so $V_C = 0$. From Eq. (19), we can obtain

$$\frac{I_{e1}}{I_{e2}} = \exp\left[\frac{e\left(V_D - V_C\right)}{k_B T_e}\right] = \exp\left(\frac{eV_D}{k_B T_e}\right)$$

$$\Rightarrow \frac{I_{\rm D}+I_{\rm si}}{I_{\rm si}-I_{\rm D}} = \exp\left(\frac{eV_{\rm D}}{k_{\rm B}T_{\rm e}}\right). \tag{20}$$

The I–V relationship of the dual probe is then obtained as

$$I_{\rm D} = -I_{\rm si}\tanh\left(\frac{eV_{\rm D}}{2k_{\rm B}T_{\rm e}}\right), \tag{21}$$

where $k_{\rm B}$ is the Boltzmann constant, and $T_{\rm e}$ is the electron temperature, which can be obtained from the slope at the origin as follows:

$$\left.\frac{{\rm d}I_{\rm D}}{{\rm d}V_{\rm D}}\right|_{I_{\rm D}=0} = \frac{eI_{\rm si}}{2k_{\rm B}T_{\rm e}}. \tag{22}$$

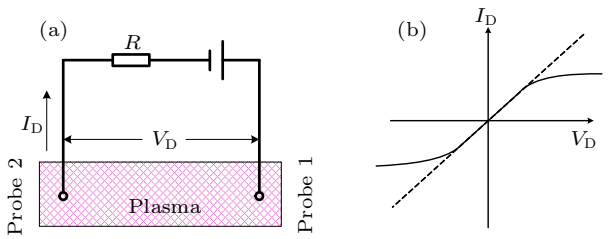


Fig. 7. Electrostatic–dual-probe diagnostic principle: (a) circuit schematic diagram and (b) volt–ampere characteristic curve.

During the experiment, an electrostatic probe measurement system was used to measure the plasma flow field parameters in a shock tube. A triangular wave voltage sweep was adopted to measure the electrostatic dual-probe volt–ampere characteristic curve. The peak-to-peak value of the triangular wave was 2.5 Vpp, frequency was 500 kHz, and the response time was less than 1 μs. The geometric shapes, areas, and materials of the two probes were all the same. The volt–ampere characteristic curve was obtained by measuring the probe current I and the scanning voltage V. Under electrically neutral conditions, the ion density is the same as the electron density. By substituting the ion saturation current collected by the probe and the electron temperature into Eq. (23), the ion density $n_{\rm i}$ can be obtained, and thus the plasma electron density $n_{\rm e}$ can be determined to be

$$I_{\rm is} = -0.605en_{\rm i}\left(\frac{T_{\rm e}}{M}\right)^{1/2}S, \tag{23}$$

where M is the ion mass, and S is the surface area of the probe.

In the calculation of the collision frequency, the post-shock pressure is needed. The pressure is obtained from a pressure sensor. When the shock wave passes through the pressure sensor, the pressure will rapidly increase from steady-state to several tens of kilopascals in a very short time. This requires the pressure sensor to have fast response, good frequency response, and anti-interference capability. In the experiment, PCB series sensors were used to measure the post-shock pressure. Owing to the axial symmetry of the shock tube flow field, the pressure sensor and probe were symmetrically placed to ensure that the pressure measurement did not interfere with the probe measurement. This ensured consistent flow field parameters and reduced the error in calculation of the collision frequency. During the experiment, the sampling rate of the electrostatic probe measurement system and the pressure measurement system is 10 MHz, with a sampling duration of 10 ms. The collision frequency is further determined according to the flow field pressure and electron temperature as follows:[19]

$$\nu_{\rm e} = \frac{5.82\times10^{12}P({\rm atm})}{\sqrt{T_{\rm e}}}. \tag{24}$$

4.2. LF experimental setup

A shock tube is a closed metal tube with an aluminum diaphragm separating low-pressure section from high-pressure section. In electromagnetic experiments, part of the metal tube in the low-pressure section is replaced with a Teflon tube to create a test section. The inner diameter of the test section is 80 mm. A 30-mm-diameter projectile model is located in the center of the test section. Inside the projectile model, an LF magnetic field probe is installed to receive LF signals, and electrostatic probes are installed at the projectile tail as shown in Fig. 8. Using both the electrostatic probes and LF method, plasma can be diagnosed, and the measurement data from the electrostatic probes can be used to verify the accuracy of LF diagnosis. During the experiment, the high-pressure section is charged with a mixture of hydrogen and oxygen. When the aluminum diaphragm breaks, a shock wave propagates toward the low-pressure section. This shock wave compresses the air around the projectile, ionization occurs, and a plasma sheath forms. The LF magnetic field probe is completely covered by the plasma, avoiding issues related to the directional transmission and diffraction shielding of LF signal.[11] Single or multiple frequencies can be chosen, and multi-frequency composite signals are transmitted simultaneously to enhance the efficiency and reliability of the experiment. The multi-frequency composite signals overlap in the time domain whereas they are discrete in the frequency domain. The mathematical expression of composite signals is

$$s(t) = \sum_{i=1}^{n}\cos(2\pi f_i t). \tag{25}$$

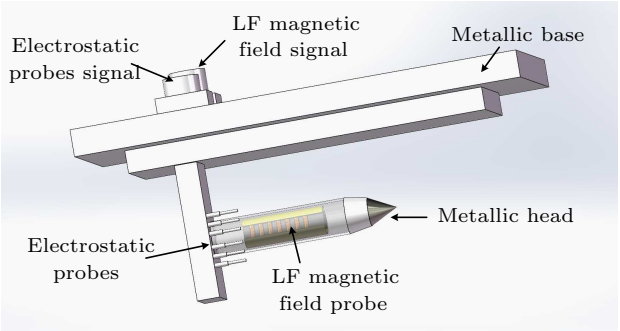


Fig. 8. Installation of electrostatic probe and LF magnetic field probe.

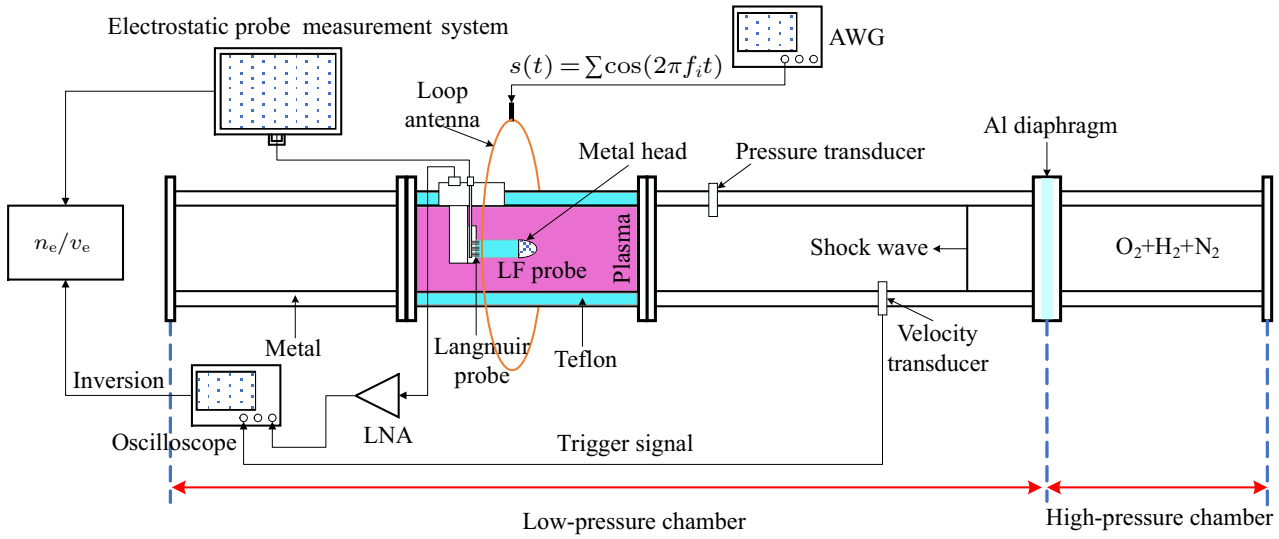


Fig. 9. Principle of LF diagnosis of shock-tube plasma.

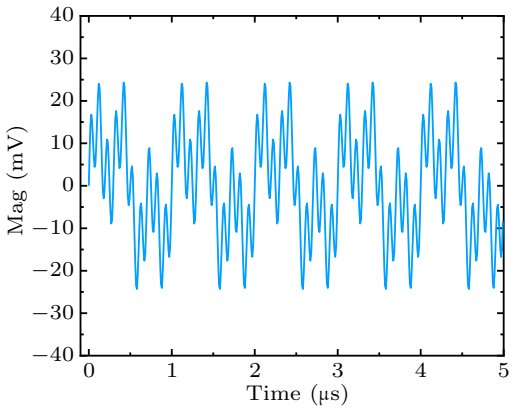


Fig. 10. Composite signal $s(t)$ waveform.

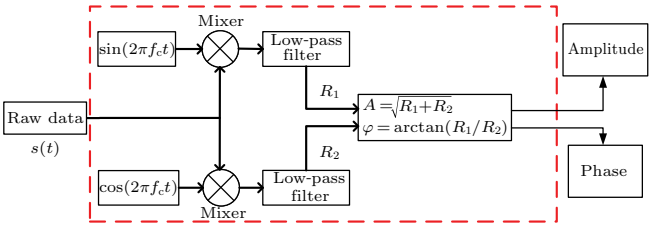


Fig. 11. Synchronous demodulation algorithm.

As shown in Fig. 9, the LF diagnosis system for the shock-tube plasma has two main parts: (i) composite signal transmission and reception and (ii) data recording and processing. In the composite signal transmission stage, an arbitrary waveform generator (AWG) (SDG2122X, Siglent) generates the multi-frequency composite signal $s(t)$, which then radiates into the surrounding area through a broadband loop antenna as the LF alternating magnetic field wave. The composite signal $s(t)$ waveform is shown in Fig. 10. The signal $s(t)$ amplitude can be adjusted through the AWG, and the maximum output amplitude of SDG2122X is 20 Vpp. The loop antenna is placed around the experimental section so that the magnetic field waves are uniformly incident on the plasma. After passing through the plasma, the signal is captured and output by the LF magnetic field probe. The received signal is amplified by a low-noise amplifier (LNA) and then acquired by using an oscilloscope (MSO54, Tektronix). The oscilloscope's sampling rate is set to 125 MHz and the sampling duration to 10 ms. Considering the short duration of the plasma, advanced triggering is adopted to provide the trigger signal before the shock wave enters the test area, thereby guaranteeing complete observation of the plasma's generation, stabilization, and ultimate dissipation. Once the acquired data are processed by the synchronous demodulation algorithm as shown in Fig. 11, the amplitude and phase information is extracted.

4.3. Experimental results and discussion

Theoretical analysis reveals that the LF alternating magnetic field waves at frequencies of 1 MHz, 3 MHz, and 10 MHz fulfill the requirements for shock-tube plasma diagnosis under typical experimental conditions. The composite signals of these three frequencies are thus used to ensure the experiment's reliability. We carry out several LF diagnostic experiments by using shock tube equipment. Photograph of the experimental scene is shown in Fig. 12. The Teflon experimental section, which is a square structure on the outside and cylindrical structure on the inside. Table 1 gives the experiment parameters for the tests.

The phase shifts measured in two shock tube experiments are shown in Fig. 13. The phase shift increases with the incident wave frequency increasing, and plasma durations are 35 μs and 75 μs respectively. Experiments are conducted to measure the temporal evolution of the flow field pressure (P) and electron temperature (T_e) following shock compression, and the results are shown in Fig. 14.

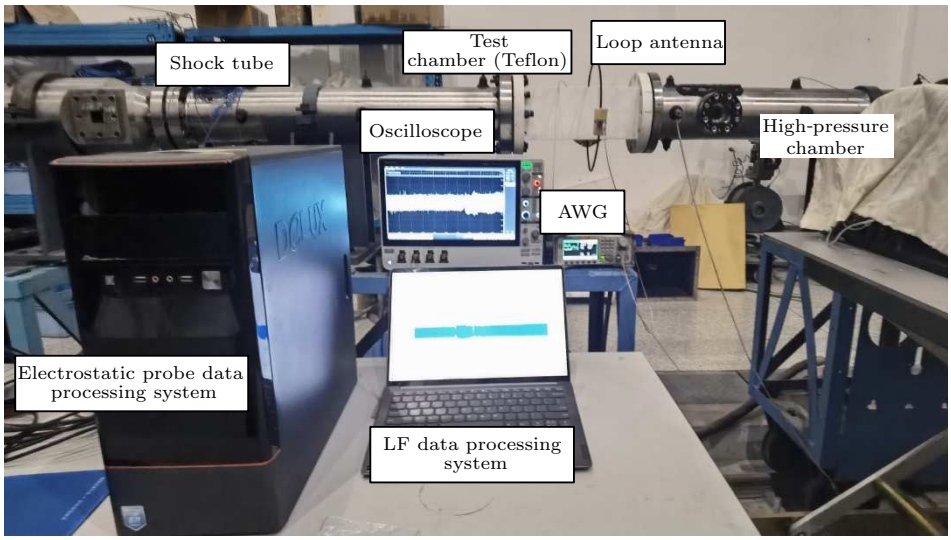


Fig. 12. Photograph of LF diagnostic experiment on shock tubes.

Table 1. LF diagnostic experiment parameters of shock tube.

Frequency (MHz)	Velocity of shock wave (km/s)	Low-pressure chamber's pressure (Pa)	Gas ratio O_2:H_2:N_2	High-pressure chamber's pressure (Pa)
1				
3	6.01	65	1.47:11.53:5	1.82×10^6
10				
1				
3	4.93	216	1.47:11.53:5	1.82×10^6
1				

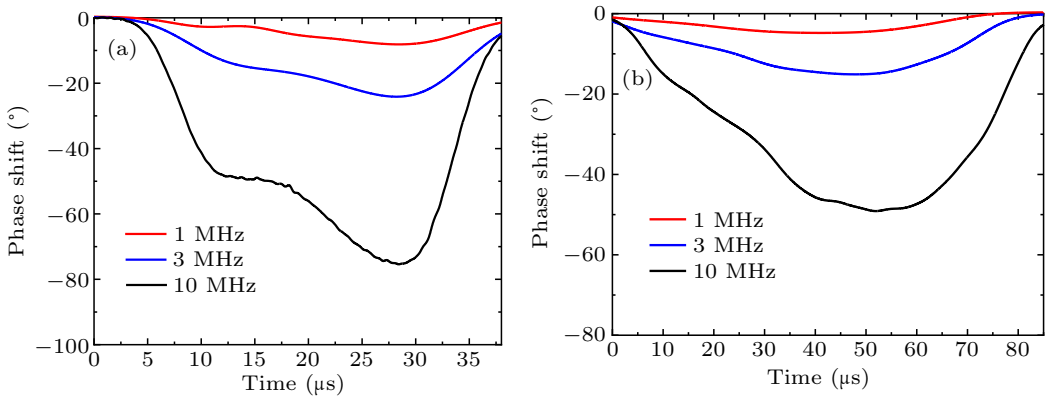


Fig. 13. Experimental phase shift of multi-frequency LF alternating magnetic field at $V = 6.01$ km/s, $P_1 = 65$ Pa (a) and $V = 4.93$ km/s, $P_1 = 216$ Pa (b).

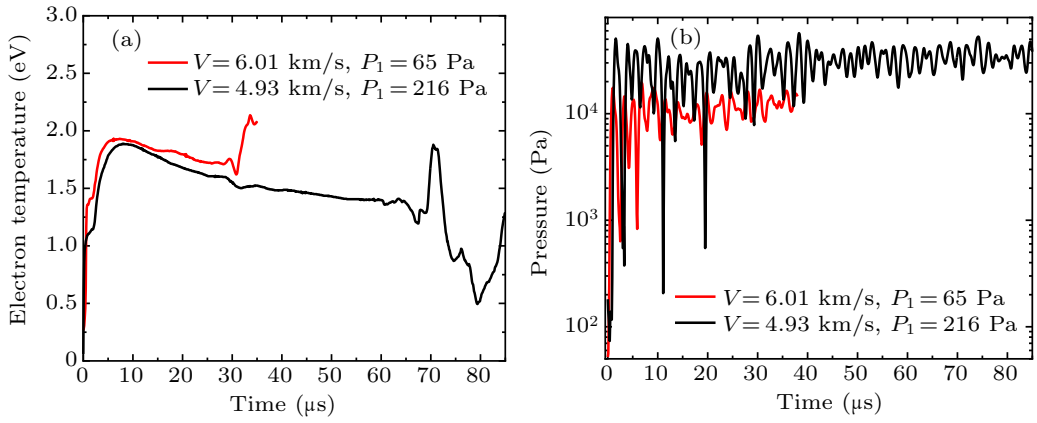


Fig. 14. Temporal evolution of (a) electron temperature and (b) flow field pressure.

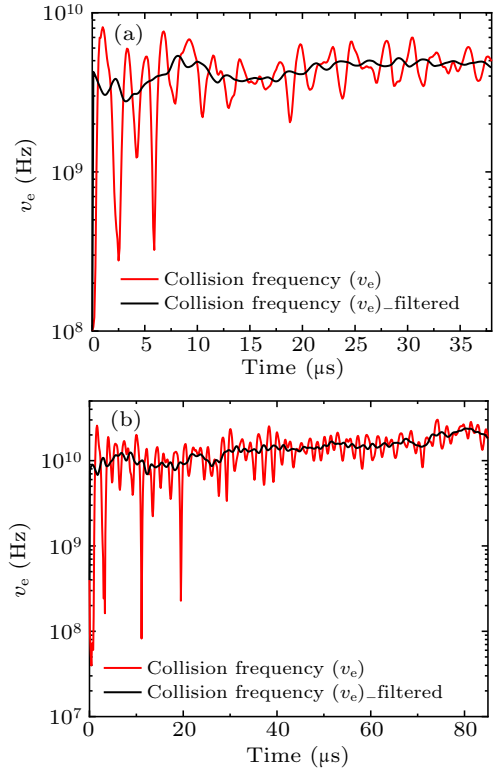


Fig. 15. Time distribution of collision frequency at $V = 6.01$ km/s, $P_1 = 65$ Pa (a) and $V = 4.93$ km/s, $P_1 = 216$ Pa (b).

Figures 15 and 16 present the distribution of collision frequency and electron density, respectively. Due to the high shock wave velocity and low pressure in the first experiment, the time required for air ionization is short, and the plasma duration is also short, resulting in a relatively flat time distribution of plasma parameters. In the second experiment, the high pressure in the low-pressure section results in a longer time required for air ionization, leading both the duration of electron density and collision frequency to increase. The plasma characteristics is determined by both the shock wave velocity and the pressure of low-pressure chamber. When the pressure of low-pressure chamber remains constant, an increase in shock wave velocity results in more significant effects of shock compression and viscous retardation, leading to a greater conversion of internal energy. As a result, the temperature behind the shock wave rises and ionization reactions intensify, thereby producing higher-electron density and higher-collision frequency. When the velocity remains constant, a lower pressure in the low-pressure section indicates thinner air, resulting in slower ionization reactions and smaller electron density and lower collision frequency, and *vice versa*. Generally, the electron temperature is more significantly affected by the shock wave speed, resulting in a higher electron temperature in the first experimental. The pressure of low-pressure chamber has a dominant effect on the post-shock pressure, resulting in a higher post-shock pressure in the second experimental condition. Since the collision frequency is directly proportional to the post-shock pressure and inversely proportional to the electron temperature, the collision frequency in the second condition is higher than that in the first experimental conditions. In the theoretical derivation, the larger the n_e/ν_e, the greater the phase shift is. The measured phase shift in the first experiment is higher than that in the second one, which is consistent with the theoretical analysis. However, since the electron density and collision frequency are affected differently by the shock wave velocity and the pressure in the low-pressure section, there is no obvious linear relationship between the n_e/ν_e and the shock wave velocity or the low-pressure section pressure. Similarly, there is no apparent linear correlation between the LF phase shift and the shock wave velocity or the low-pressure section pressure.

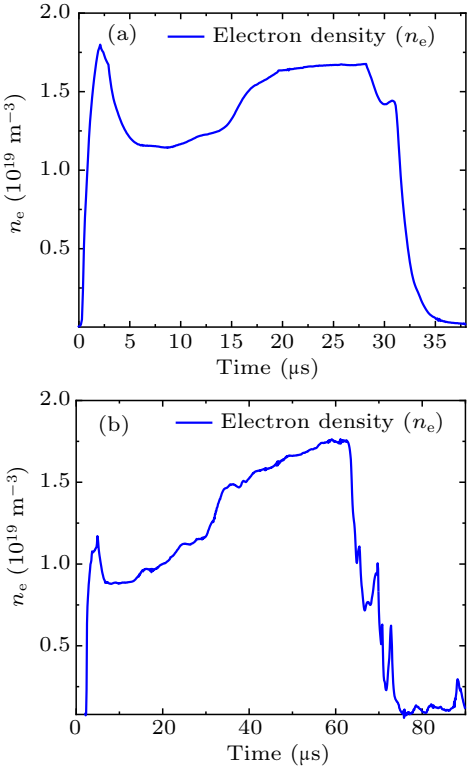


Fig. 16. Electron density obtained by electrostatic probes at $V = 6.01$ km/s, $P_1 = 65$ Pa (a) and $V = 4.93$ km/s, $P_1 = 216$ Pa (b).

Figure 17 shows the diagnosis results of n_e/ν_e, corresponding to n_e/ν_e values ranging from 1×10^9 to 1×10^{10}, with a relatively uniform distribution during plasma stabilization. It is seen that the results obtained by using the LF method and the electrostatic probes are relatively consistent during the period when plasma is stabilized. However, the diagnostic results vary with frequency. This is attributed to the induced current always following the path of least resistance, where higher incident frequencies exhibit a stronger skin effect. The actual inductive path is thus longer than the inverse solution path, leading to an overestimation of the 10-MHz calculation result. Accordingly, the induction paths of 1 MHz and 3 MHz are the same to a great extent, resulting in a higher consistency between the diagnosis resultsof these two frequencies. However, the n_e/ν_e diagnosed results are in relatively poor agreement in Fig. 17(b). This can be attributed to the slow shock wave speed, the high pressure in the low-pressure section, and the

extended time required for air ionization. After the shock wave arrives, the electron density continues to rise. The plasma will fill in the shock tube through its diffusing from the center to the surroundings, and as the plasma with continuously varying parameters spreads outwards, its spatial distribution becomes more and more non-uniform. Conversely, figure 17(a) shows that the plasma parameters are more consistent and the spatial distribution remains more uniform after diffusion.

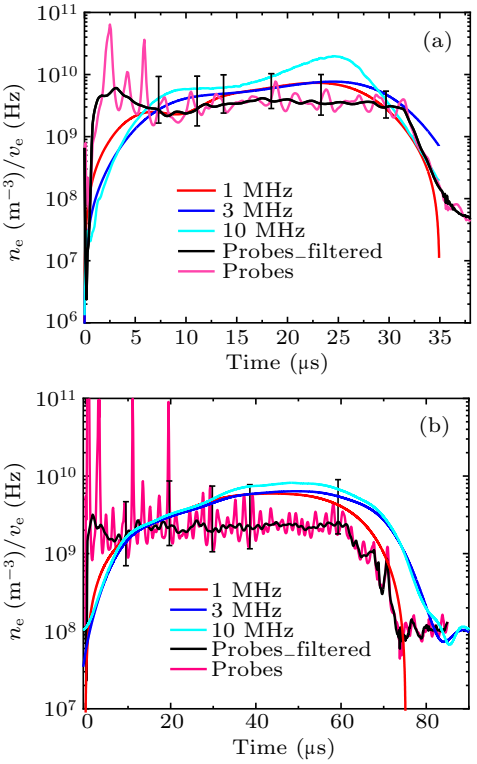


Fig. 17. Variations of n_e/v_e with time obtained by the electrostatic probe method and LF method at $V = 6.01$ km/s, $P_1 = 65$ Pa (a) and $V = 4.93$ km/s, $P_1 = 216$ Pa (b).

In the LF method, the phase shift of the LF alternating magnetic field is used to measure the n_e/v_e. The phase shift accuracy depends on the accuracy of the data acquisition oscilloscope and the LF magnetic field probe. The oscilloscope (Tektronix MSO54) has high stability, with a bandwidth (calculated rise time) of 500 MHz (800 ps), a vertical resolution of 12 bits, automatic calibration and calibration functions, and the phase stability of better than $\pm 0.1^\circ$. A standard magnetic antenna (EM-6992, Electro-Metrics Corporation) is used to calibrate the LF magnetic field probe. The experimental data collected include phases with and without plasma. Subtracting the two phases yields the phase shift caused by the plasma, which avoids the errors caused by the experimental environment. Therefore, the LF experimental equipment and operational errors can be ignored. The electrostatic probe diagnoses the electron density and temperature at a fixed point in space. The collision frequency is calculated by using the electron temperature and pressure. The symmetric placement of the probe and pressure sensor ensures consistent flow field and reduces calculation errors. A mean filtering method is introduced to process the n_e/v_e, and the original data and confidence intervals of the probe are provided. It is necessary to normalize the sampling times of the two diagnostic methods to ensure time consistency when making comparisons.

The differences in diagnostic results between the LF method and the electrostatic probe method lie mainly in the rising time of the plasma, which are caused by different physical mechanisms. The electrostatic probe method measures the time-varying curve of the electron density and collision frequency at a point in the surface normal direction of the vertical projectile model. Upon breaking through the aluminum diaphragm, the high-pressure mixture gas generates a shock wave that travels downstream towards the low-pressure section. This shock wave compresses the air, leading to its ionization and the formation of a two-zone plasma. As the shock wave advances towards the low-pressure section, it is accompanied by intense light radiation characteristics. Its velocity is significantly higher than that of the shock wave, enabling ions and electrons generated by the light radiation to reach the surface of the electrostatic probe more rapidly. This results in a step increase in the measured electron density and temperature. At this time, the model is not completely enveloped by the plasma, which is insufficient to affect the change in the LF alternating magnetic field. As the shock wave arrives, the plasma gradually fills the shock tube, and the LF phase shift gradually changes, resulting in a gradual increase in the LF diagnostic results. Once the plasma has filled the shock tube, the diagnostic results of the two methods converge. During the plasma's stable stage, the discrepancies arise from the non-uniform spatial distribution of plasma within the shock tube and the incomplete coincidence between the LF diagnostic path and the probe diagnostic position. In the high-pressure section, a hydrogen–oxygen mixture gas is introduced, and during the plasma's disappearance stage, H_2O molecules and other impurities generated when electrons and ions begin to recombine. The 2-zone gas is no longer a pure plasma, resulting in discrepancies between the results from the electrostatic probe and LF method. Nevertheless, the LF diagnostic results fall within the confidence interval of the electrostatic probe, initially suggesting the viability of the LF diagnostic method.

Although LF diagnostic method can directly diagnose the n_e/v_e, it is difficult to directly obtain the separate distributions of the electron density or collision frequency. When a parameter is known, substituting it into the n_e/v_e measured by the LF method can determine the value of the other parameter. This necessitates that the spatial location pertaining to the provided parameters must align with that of the LF diagnosis. The LF method directly measures the ratio between the plasma loop average electron density and collision frequency. However, existing diagnostic methods are unable to obtain parameters on such a loop path, which necessitates a uniform spatial distribution of the plasma to ensure identical parameters on different paths. In this case, the accuracy of the other parameter obtained by substituting one parameter into the n_e/v_e is

higher. From another perspective, the LF diagnostic method can be combined with other techniques to diagnose plasmas, allowing for the acquisition of electron density and collision frequency distributions. The application range of LF diagnostic method encompasses a series of common plasma source parameter ranges, making the combined diagnostic approach suited for parameter diagnosis in various plasma sources such as small-scale shock tubes, inductively coupled plasma wind tunnels, and others.

5. Conclusions

A non-contact LF diagnostic method is proposed in order to meet the diagnosis requirements of the scaled-model plasma sheath in a shock tube. This method enables the direct measurement of the ratio of the electron density to the collision frequency of the plasma surrounding the model. The relationship between the LF phase shift and the plasma parameters is derived by using equivalent circuit theory, establishing the inversion model for the ratio of electron density to collision frequency. The LF diagnostic experiments are conducted in a shock tube, and the inversion results are relatively consistent with those of the electrostatic probe under the same experimental conditions. This preliminary validation confirms the effectiveness of the LF diagnostic method.

The LF inversion model under different plasma envelopes, such as rectangular, spherical, and cylindrical shapes, is analyzed. Since the LF method directly measures the ratio between the plasma loop average electron density and collision frequency, it is more suitable for enveloped plasma. Further inference suggests that the LF method has the potential application in diagnosing the plasma with arbitrary enveloping shapes. Meanwhile, the applicable range of the LF method on a given plasma scale is analyzed, where the electron density can exceed 1×10^{20} m^{-3}, the collision frequency is less than 1 GHz, and the ratio of the electron density to the collision frequency exceeds 1×10^{11}. This method can be used for high-density enveloping plasma diagnosis.

The ratios of electron density to collision frequency in the two typical experimental conditions are both on the order of 10^{10}, and the time distribution is relatively uniform. Owing to non-uniform spatial distribution of plasma, there is a deviation between the actual induction path and the calculated path, results in significant calculation errors. When the plasma exhibits a uniform spatial distribution, and one parameter, either the electron density or the collision frequency, is known, the LF method can be used to derive the other parameter. Further research will focus on the influence of plasma spatial non-uniformity and explore the combined diagnostic approaches involving LF method.

Acknowledgements

Project supported by the National Natural Science Foundation of China (Grant Nos. 52107162 and 12202479), the Science and Technology Projects of Shaanxi Province, China (Grant Nos. 2022CGBX-12 and 2022KXJ-57), and the Science and Technology Projects of Xi'an City, China (Grant Nos. 23KGDW0023-2022 and 23GXFW0011).

References

[1] Scharfman W E 1965 *The use of Langmuir probes to determine the electron density surrounding re-entry vehicles* (Washington DC: NASA)
[2] Guo S S, Xie K, Sun B, Xi R Y and Liu Y 2021 *Plasma Sci. Technol.* **23** 075401
[3] Sakthi B G and Aravind R S 2023 *Int. J. Impact. Eng.* **172** 104406
[4] Lyu X T, Jiang C X, Feng W and Ge N 2017 *IEEE Trans. Plasma Sci.* **45** 2050
[5] Sun Q, Cui W, Li Y H, Cheng B Q, Jin D and Li J 2014 *Chin. Phys. B* **23** 075120
[6] Man L, Deng H C, Wu Y, Yu X L and Xiao Z H 2022 *Acta Phys. Sin.* **71** 035203 (in Chinese)
[7] Xie K 2014 *Study On Plasma Sheath Reproducing Technology and Related Issues in EM-Wave Propagation Experiment*, Ph.D Thesis (Xi'an: Xidian University) (in Chinese)
[8] Liu D L, Li X P, Xie K and Liu Z W 2015 *Phys. Plasmas* **22** 102106
[9] Xie K, Guo S S, Sun B, Quan L and Liu Y 2019 *Phys. Plasmas* **26** 073509
[10] Sun B, Xie K, Liu Y, Zhang Y J, Guo S S and Ma P 2022 *IEEE Trans. Plasma Sci.* **50** 102106
[11] Xie K, Sun B, Guo S S, Quan L and Liu Y 2019 *Rev. Sci. Instrum.* **90** 073503
[12] Guo S S, Xie K, Sun B and Liu S W 2020 *Plasma Sci. Technol.* **22** 125301
[13] Guo S S 2021 *An Approach to Plasma-Spatiotemporal-Electromagnetic-Regulation-Based Enhanced Magnetic Window Methods and Its Experimental Researches*, Ph.D Thesis (Xi'an: Xidian University) (in Chinese)
[14] Liu D L 2015 *Study on the Low-frequency EM Wave Transmission Characteristics under Plasma sheath and Blackout Mitigation by E × B*, Ph.D Thesis (Xi'an: Xidian University) (in Chinese)
[15] Ivaro S V, Federico B, Victor D, Julien J, Denis P, Eduardo A and Mario M 2023 *Plasma Sources Sci. Technol.* **32** 014002
[16] Yu P C, Liu Y, Liu X Q and Lei J H 2022 *Phys. Plasma* **29** 093508
[17] Ming Z J, Lan T, Li H, Xie J L, Liu A D and Liu W D 2015 *Acta Phys. Sin.* **64** 115201 (in Chinese)
[18] Lan H, Shi T H, Yan N, *et al.* 2023 *Plasma Sources Sci. Technol.* **25** 075105
[19] Banks P M and Kockarts G 1973 *Aeronomy: Part A* (New York: Academic)
[20] Wu M X, Tian D Y, Tang P, Tian J, He Z Y and Ma P 2022 *Acta Phys. Sin.* **71** 115202 (in Chinese)
[21] Zhao C W, Li X P, Liu Y M, Liu D L, Sun C, Ma G L, Tian L S and Bao W M 2022 *Plasma Sources Sci. Technol.* **31** 015007
[22] Tian J, Ma P, Chen B, Hu H Q, Zeng B, Li L T and Tang P 2022 *Plasma Sci. Technol.* **24** 045505
[23] Ma G L, Liu Y M, Zhao C W, Sun C and Bao W M 2022 *Plasma Sci. Technol.* **24** 075501
[24] Varavin M, Varavin A, Naydenkova D, Zajac J, Zacek F, Nanobashvili S, Panek R, Weinzettl V, Bilkova P, Kovarik K, Jaulmes F, Farnik M, Imrisek M and Bogar O 2019 *Fusion Eng. Des.* **146** 1858
[25] Ginzburg (translated by Qian S X) 1978 *Propagation of electromagnetic wave in plasma* (Beijing: Science Press) pp. 5–9 (in Chinese)
[26] Yang S Y 2006 *Electromagnetic Shielding Theory and Practice*, (Beijing: National Defense Industry Press) pp. 136–138 (in Chinese)
[27] Wheeler H A 1958 *Proc. IRE* **46** 1595
[28] Miller D A and Bridges J E 1968 *IEEE Trans. Electromagn. Compat.* **10** 52